PROSPECTING the Moon: Numerical Simulations of Temperature and Sublimation Rate of a Cylindric Sample

M.Formisano[a,*], M.C. De Sanctis[a], S. De Angelis[a], J.D. Carpenter[b], E. Sefton-Nash[c]

[a] *IAPS-INAF, Via del Fosso del Cavaliere 100, 00133 Rome (Italy)*
[b] *ESA-ESTEC, Keperlaan, 1, 2401, AZ, Noordwijk, The Netherlands*
[c] *ESA-ESTEC, Keplerlaan 1, 2201 AZ Noordwijk, The Netherlands*

Abstract

The goal of the ESA Luna 27/PROSPECT instrument [1] is to extract and characterize a regolith sample from the lunar south polar region, investigating its physical and chemical properties. The main target is to characterize the abundance and distribution of water ice and other volatiles so the challenge is to preserve volatiles in samples during the drilling transfer and analysis. In this work we provided numerical simulations in order to predict the expected ice sublimation rates and inform the system's development. Simulations are characterized by different initial boundary conditions as well as thermodynamic parameters and carried out on a cylinder representing a lunar regolith sample of the south polar region.

Keywords: `Moon, sublimation, water ice, thermal modeling`

1. Introduction

The Moon represents a potential source of ice for its cold trapped water at the poles [2]. However, there is a great uncertainty linked to the distribution and abundance of this ice as well as the local environment associated with it. Neutron measurements from orbit [3] have revealed an hydrogen enhancement,

*Corresponding author
Email address: `michelangelo.formisano@inaf.it` (M.Formisano)

compatible with the presence of water within 1 meter (approximately) from the surface and also bolometric temperature measurements indicate that the water ice is stable within 1 meter from the surface. These peculiarities suggest the depth at which the ESA PROSPECT system will analyze material, arriving down to 2 meter beneath the surface at the poles [1]. The principal aims to achieve for PROSPECT are [1]: the drilling and extracting of samples from depths of up 2 meters, extracting water, oxygen and other elements of interest from a resource point of view; the identification of these elements, quantifying the abundances of these species and characterizing the isotopes. The PROSPECT package consists of the drill (ProSEED) and of a chemical laboratory (ProSPA) in which the sample taken by the drill is heated to extract cold trapped volatiles that will be analysed [4]. The launch of PROSPECT to the Moon will be on the Russian Luna 27 mission and the landing site will be the south polar region [1]. The flight is scheduled in 2022-2023 time frame.

It is very crucial to estimate the expected ice sublimation rates and establish if the volatiles are preserved or not during the drilling transfer and analysis. Numerical simulations are here carried on to provide an answer to these questions. By applying a 3-D finite element method (FEM), we performed simulations on a cylinder representing a lunar regolith sample in the south polar region. The paper is structured as follow: a discussion about the numerical method with the initial and boundary conditions adopted in Section II, the discussion of the results in Section III and finally the conclusion of the work in Section IV.

2. Numerical Method

2.1. Geometry and Initial Conditions

The lunar sample modeled in this work is a cylinder of 3 mm of diameter and 6 mm height [5] (see Fig.1), approximating the expected sizes of the PROSPECT oven of the chemical laboratory (ProSPA). The sample is covered with a triangular mesh (864 triangular elements), whose maximum element size is 0.048 mm. The number of degrees of freedom is 9188. All sides have fixed tem-

Model	Water ice content [vol.%]	Boundary Temperature [K]
A1	0.1	148
A2	0.1	173
A3	0.1	223
B1	1	148
B2	1	173
B3	1	223
C1	10	148
C2	10	173
C3	10	223

Table 1: Scenarios analyzed in this work, differing in water ice content and boundary temperatures.

perature during all the time of simulation: this boundary temperature ranges from 148 K to 223 K. The choice of these temperatures as boundary conditions have been suggested by the thermal designer of the oven. The sample is initially at 123 K and is modeled as a mixture of ice (0.1 to 10 vol.%) and regolith. In Table 1 we report the models under study.

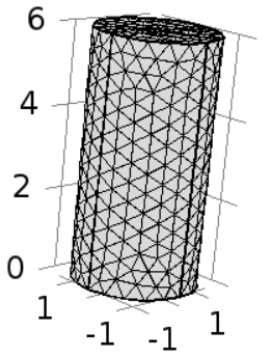

Figure 1: Cylindrical sample with a mesh made of free triangles. The radius of the cylinder is 1.5 mm while the height is 6 mm. The ice is lost only through the bottom side.

Physical Quantity	Value	Unit	Reference
Porosity	0.5	- -	this study
Regolith specific heat	760	J kg^{-1} K^{-1}	[6]
Regolith thermal conductivity	0.1	W m^{-1} K^{-1}	this study
Regolith density	1660	kg m^{-3}	[6]
Ice specific heat	7.037 T + 185	J kg^{-1} K^{-1}	[7]
Ice thermal conductivity	567/T	W m^{-1} K^{-1}	[8]
Ice density	950	kg m^{-3}	this study
Entalphy of sublimation	51983.9 - 20.0904T	J mol^{-1}	[9]

Table 2: Physical parameters used in the simulations of this work.

2.2. Equations

We used a 3-D finite element method (FEM) with the software COMSOL Multiphysics (www.comsol.com) in order to solve a modified version of the heat equation, in which we introduced a term ($Q(r,T)$) related to the energy needed for water ice sublimation from the sample [10, 11, 12, 13, 14, 15, 16, 17]:

$$\rho(r)c(r,T)\frac{\partial T}{\partial t} = \vec{\nabla}\cdot(K(r,T)\vec{\nabla}T) + Q(r,T) \tag{1}$$

where T is the temperature, t the time, $\rho(r)$ the density, $c(r,T)$ the specific heat, and $K(r,T)$ the thermal conductivity. Heat transfer occurs only by conduction since convection is negligible due to the small temperature gradients involved as well as the characteristic size of the sample. Radiation is also neglected. A mass conservation equation controls the water vapour emission:

$$\frac{\partial \rho}{\partial t} = -\vec{\nabla}\cdot\vec{J} + \tilde{Q}(r,T), \tag{2}$$

where $\tilde{Q}(r,T)$ is the gas source term due to sublimation process. By using the Fick law, the diffusion flux vector ($\vec{J}$) can be expressed as

$$\vec{J} = -D(T)\vec{\nabla}P, \tag{3}$$

which is valid in a quasi-stationary regime and where P is the partial pressure of the water vapor and $D(T)$ is the gas diffusion coefficient. By evaluating

the Knudsen number we can define the appropriate diffusion coefficient. The definition of Knudsen number is (e.g. [10, 14]):

$$K_n = \frac{\lambda}{2r_p}, \tag{4}$$

where r_p is the pore radius and λ is the mean free path, defined as [18]:

$$\lambda = \frac{\mu}{\sqrt{(}2)\pi d^2 Na\rho}, \tag{5}$$

where μ is the water molar mass (0.018 kg per mole), d is the water molecular diameter, Na is the Avogadro's number, and ρ is the density of the water vapour. If we assume $d = 5 \times 10^{-10}$ m [10] and $r_p = 10^{-4}$ m [14], the mean free path is of the order of 10^{-1} m and the diffusion regime is the Knudsen regime in which the escaping velocity of the gas is simply the mean thermal velocity:

$$v = \sqrt{\frac{8RT}{\pi\mu}}. \tag{6}$$

Using the Equation (3) we can write the Equation (2) as:

$$\frac{\partial\rho}{\partial t} = \vec{\nabla} \cdot \left(D(T)\vec{\nabla}P\right) + \tilde{Q}(r,T). \tag{7}$$

The diffusion coefficient is defined as:

$$D(T) = r_p\sqrt{\frac{\pi}{2\mu RT}}. \tag{8}$$

Assuming the water vapour as a perfect gas, we can deduce an expression for $\tilde{Q}(r,T)$. So from the Equation (7):

$$\tilde{Q}(r,T) = \frac{1}{R_{spec}T}\frac{\partial P}{\partial t} - \vec{\nabla} \cdot \left(D(T)\vec{\nabla}P\right), \tag{9}$$

where R_{spec} is the specific gas constant defined as the ratio between the universal gas constant (R) and the molar mass (μ). This term is linked to the energy absorbed by the sample ($Q(r,T)$):

$$Q(r,T) = -\phi L(T)\tilde{Q}(r,T), \tag{10}$$

where ϕ is the porosity and $L(T)$ is the latent heat of sublimation. Finally, using Equations (9) and (10) we can write the heat equation in the form (assuming

local thermodynamic equilibrium):

$$\left(\rho c + \frac{\phi L(T)}{RT}\frac{\partial P_{sat}(T)}{\partial T}\right)\frac{\partial T}{\partial t} = \vec{\nabla}\cdot\left(K(T)\vec{\nabla}T\right) + \phi L(T)\vec{\nabla}\cdot\left(D(T)\vec{\nabla}P_{sat}\right). \quad (11)$$

Density, specific heat and thermal conductivity are weighted as follow:

$$\rho_{mix} = vf_{ice}\rho_{ice} + vf_{reg}\rho_{reg}, \quad (12)$$

$$c_{p,mix} = mf_{ice}c_{p,ice} + mf_{reg}c_{p,reg}, \quad (13)$$

$$K_{mix} = vf_{ice}K_{ice} + vf_{reg}K_{reg}, \quad (14)$$

where vf_{ice} and vf_{reg} are the volumetric percentage of ice and regolith (porosity corrected), while mf_{ice} and mf_{reg} are the mass percentages. The water ice saturation pressure is defined as [19]:

$$P_{sat} = exp\left(9.550426 - \frac{5723.265}{T} + 3.53068ln\left(T\right) - 0.00728332T\right), \quad (15)$$

valid for $T > 110$ K. In order to estimate the water ice sublimation rate, we use the following classical expression [9]:

$$\Gamma = P_{sat}\sqrt{\frac{\mu}{2\pi RT}}, \quad (16)$$

where Γ is expressed in kg m^{-2} s^{-1}. In Table 2 the principal physical parameters adopted in this work are reported.

3. Results

In the following sections we will report the results of our numerical simulation for the different physical cases under investigation. We start with the scenario A, characterized by the lowest value of ice volume percentage (0.1 vol.%) and then we will discuss how the results change with increasing ice content (scenario B - 1 vol.%, scenario C - 10 vol.%). For each case we will report the sublimation rate as a function of the time of simulation. The rate of sublimation is computed by using the Equation (16) calculated with the mean temperature at each time step and by considering that the ice is loss only through the bottom side of the sample, i.e. the side where the drill works.

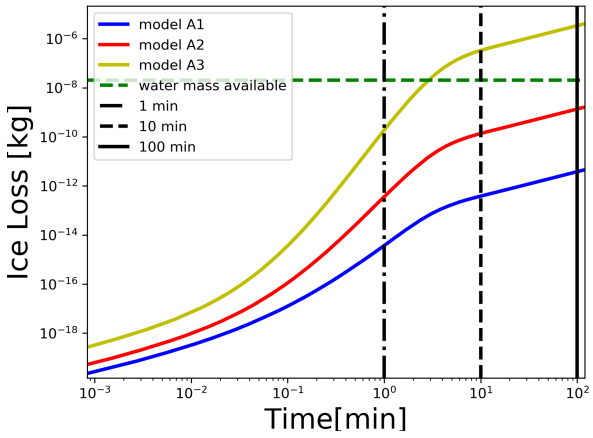

Figure 2: Scenario A: ice loss plot vs simulation time expressed in minutes. Horizontal green dash line represents the available water mass and the intersection between this line and the sublimation curve (ice loss during the simulation) gives an estimation of the time needed to consume all the available water ice.

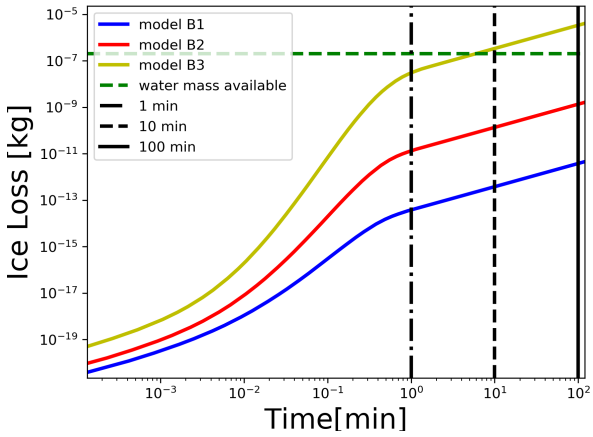

Figure 3: Scenario B: ice loss plot vs simulation time expressed in minutes. Horizontal green dash line represents the available water mass and the intersection between this line and the sublimation curve (ice loss during the simulation) gives an estimation of the time needed to consume all the available water ice.

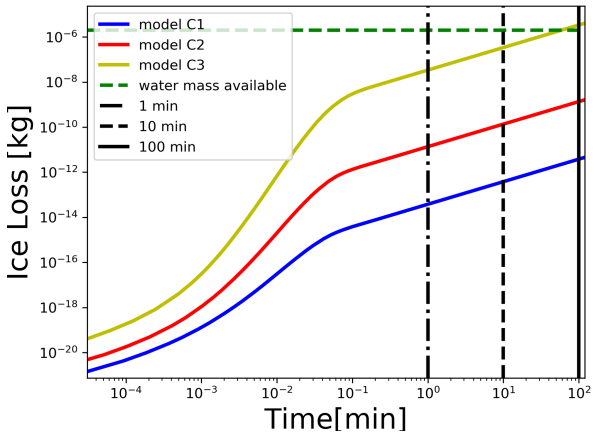

Figure 4: Scenario C: ice loss plot vs simulation time expressed in minutes. Horizontal green dash line represents the available water mass and the intersection between this line and the sublimation curve (ice loss during the simulation) gives an estimation of the time needed to consume all the available water ice.

3.1. Scenario A

Scenarios A are characterized by a low volumetric percentage of ice of 0.1 vol.% and boundary temperatures ranging from 148 K to 223 K. In Fig.2 we report the results concerning this scenario. The total time of simulation is 120 minutes. The blue (model A1), red (model A2) and yellow (model A3) curves represent the ice loss during the simulation, while the black vertical lines refer to 1, 10 and 100 min from the beginning of simulation. The intersection with the ice loss curve gives an estimation of the volumetric percentage of ice lost at those times. The horizontal green line indicates the initial available water mass of ice, which in this case is 2×10^{-8} kg. The results of this scenario are summarized in Tab.3. We observe that a boundary temperature slightly higher than the sample temperature lead to a very negligible ice mass loss, even after 100 minutes from the beginning of the simulation. The mass loss begins to be significant in the A2 case, characterized by 173 K on the sides, when a 7% of the total is lost after 100 minutes from the beginning of the simulation. If the boundary temperatures are increased to 223 K, the complete loss of the water ice is reached in a very short

Model	Mass loss [kg] after 1 min	Mass loss [kg] after 10 min	Mass loss [kg] after 100 min
A1	3.9×10^{-15}	4.8×10^{-13}	4.2×10^{-12} [0.02%]
A2	5.6×10^{-13}	1.3×10^{-10} [1%]	1.5×10^{-9} [7%]
A3	2.3×10^{-10} [1%]	TOTAL	TOTAL

Table 3: Scenario A: Mass of ice loss (in kilograms) after 1, 10 and 100 minutes from the beginning of the simulation. In brackets the percentage loss (only for the cases with an ice loss $> 0.01\%$). Boundary temperatures range from 148 K (A1) to 223 K (A3). Available initial mass of ice is 2×10^{-8} kg.

time, about 3 minutes from the start. The change in curvature in each model output plot reflects the behaviour of the mean temperature (see Appendix), in particular it occurs when an uniform temperature is reached inside the whole domain. Due to the very reduced time of existence of the ice, it would be very difficult to analyse the volatiles in such a sample. The time needed to sublimate the whole ice content is identifiable as the intersection between the sublimation curve and the horizontal green line. In the last phase of the simulation we have a quasi flat plot, since the steady loss state is reached.

3.2. Scenario B

Models of Scenario B are characterized by a volume percentage of ice of 1% which means an available ice mass of 2×10^{-7} kg. In the case of the lowest boundary temperatures (B1, 148 K) the sublimation rate is negligible after the total time of simulation and this is very similar to what happens in the case of a boundary temperature of 173 K (B2) after 10 minutes of simulation. In this last case (B2) a very small quantity of ice ($\simeq$1% of total) is lost after 100 minutes. As expected, the situation changes as the temperatures of the sides are increased (B3, 223 K): after 1 minute, the loss is of 15% until it becomes total after 3.5 minutes from the beginning of the simulation. Results are shown in Fig.3 and summarized in Table 4.

3.3. Scenario C

The last models considered in our simulations are characterized by an ice volume percentage of 10% which corresponds to an available initial mass of ice

Model	Mass loss [kg] after 1 min	Mass loss [kg] after 10 min	Mass loss [kg] after 100 min
B1	3.8×10^{-14}	4.6×10^{-13}	4.1×10^{-12}
B2	1.7×10^{-11} [0.01%]	1.9×10^{-10} [0.1%]	1.5×10^{-9} [0.8%]
B3	3.7×10^{-8} [15%]	TOTAL	TOTAL

Table 4: Scenario B: Mass of ice loss after 1, 10 and 100 minutes from the beginning of the simulation. In brackets the percentage loss (only for the cases with an ice loss > 0.01%). Boundary temperatures range from 148 K (B1) to 223 K (B3). Available initial mass of ice is 2×10^{-7} kg.

Model	Mass loss [kg] after 1 min	Mass loss [kg] after 10 min	Mass loss [kg] after 100 min
C1	3.6×10^{-14}	5.1×10^{-13}	4.2×10^{-12}
C2	1.5×10^{-11}	1.5×10^{-10}	1.5×10^{-9} [0.07%]
C3	4.3×10^{-8} [2%]	4.6×10^{-7} [23%]	TOTAL

Table 5: Scenario C: Mass of ice loss after 1, 10 and 100 minutes from the beginning of the simulation. In brackets the percentage loss (only for the cases with an ice loss > 0.01%). Boundary temperatures range from 148 K (C1) to 223 K (C3). Available initial mass of ice is 2×10^{-6} kg.

of 2×10^{-6} kg. As in the previous case, a temperature of the sides of 148 K (C1) or 173 K (C2) does not lead to very significant loss of ice during all the simulation time. Only in case C3, a temperature of 223 K on the sides, leads to a loss of ice of 2% after 1 minute, 23% after 10 minutes, and reaching the complete loss after 30 minutes from the beginning of our simulation. Results are shown in Fig.4 and summarized in Table 5.

3.4. Influence of Thermal Conductivity

By using B3 model as test case, we analyzed the influence of the thermal conductivity on the sample temperature and consequently on the sublimation rate. For this purpose, we tested three values of regolith thermal conductivity, which is the main component of our sample: 0.1, 0.01 and 0.001 W m^{-1} K^{-1}. What we note from the Fig.5 is that the three curves after an initial different behavior, converge in the same plot due to the fact that the stationarity is reached quickly in such a small sample. So the time needed to remove all the initial available ice is the same for the three simulations.

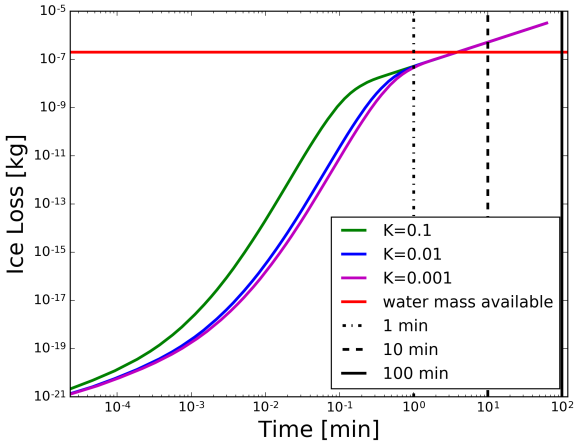

Figure 5: Model B3: Influence of the thermal conductivity on the sublimation rate.

3.5. Validation of the numerical model: a comparison with an experimental case

Even though the literature concerning sublimation of water ice of lunar regolith sample is limited, in order to validate the numerical model adopted for the simulations of this work, we developed a numerical simulation that reproduces the experiment conducted by [20], discussed in the Section 6 of their paper. They prepared a pure ice sample in a cylindrical container (13 x 8 cm) held at a temperature between 203 K and 206 K, at a pressure of $(4 \pm 1) \times 10^{-4}$ Torr with a run time of about 12 h. They measured a mass loss of 37.5±0.7g. We performed two simulations in which the pure ice cylinder, of the same size of [20], is heated at 203 K and 206 K. In Fig.6 the numerical results are reported, i.e. the ice loss (in grams) during the simulations. At the end of the simulation, in the lowest temperature case (203 K) the ice loss is of 58 g, while in the highest temperature case (206 K) the ice loss is of 78 g. We are assuming the ice loss only through one side of the cylinder, since in [20] it is not specified the emitting area. As discussed also by [21], if the ice is "dirty", mixed for example with regolith, we note a lowering of the vapor pressure and consequently a slowing of the sublimation rate. Another test to validate our model is to reproduce one of the experiment of [22], which analysed the sublimation of water ice (and

the D/H fractionation) at low temperatures in vacuum. We simulated a pure water ice cylinder (0.5 cm of radius and 2 cm height), approximately the volume occupied by the water ice in the glass u-shaped trap of the experiment of [22]. The temperature is set at about 200 K and the pressure at 10^{-3} mbar. Our simulations suggest that the water ice that sublimates after 1 minute is about 3% (against the 5% of [22]) while after 10 minutes the loss by sublimation is about 40% (against the 33% of [22]). In Fig.7 we show the sublimation curve vs time of this simulation. We note a good agreement between these experimental results and our numerical predictions.

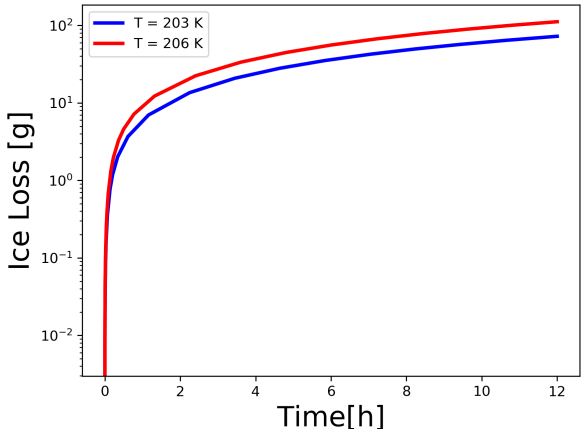

Figure 6: Results of the numerical simulations that reproduce one of the experiment found in [20]. Two boundary temperatures (203 K and 206 K) are adopted.

4. Conclusions

The numerical simulations carried out in this work show that small temperature gradients between the sample (at temperature of 123 K) and the lateral sides do not lead to a significant loss of water ice after 100 minutes. This fact is independent of the initial available volumetric concentration of water ice. No preservation, after 100 minutes, of water ice is obtained if the temperature of the boundaries is 223 K. In this last case, the mission sampling process should

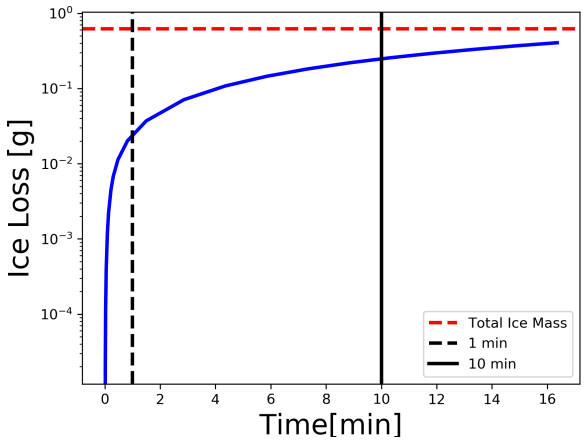

Figure 7: Results of the numerical simulations that reproduce one of the experiment found in [22]. A temperature of about 200 K at the boundaries is applied.

not exceed 10 minutes in order to have an available significant quantity of water ice. Water ice loss is influenced by the thermal conductivity only in the very early stages of the simulations. We can observe that after 1 minute, no changes in the sublimation rate occur if we use different values of thermal conductivity for the sample. As also suggested by the experiments of [22], the PROSPECT working temperature guideline of about 128 K is such to not have a major loss of water ice during the drilling and the analysis phase. Our numerical results are also in agreement with the analytical calculations of previous studies (e.g. [21]). The preservation of water ice on lunar subsurface could represent a very important *in-situ* resource for future space missions.

5. Acknowledgments

This work is supported by the Agenzia Spaziale Italiana (ASI) and carried out for the PROSPECT User Group (PUG) in support of ESA's PROSPECT package.

Appendix: Temperature Profiles

In Fig.8 we report the mean temperature vs time profiles for each scenarios we analyzed. Black vertical lines marks 1, 10 and 100 minutes from the beginning of simulations.

References

[1] J. D. Carpenter, R. Fisackerly, S. Aziz, B. Houdou, Exploring Cold Trapped Volatiles from Stationary Landers and Mobile Rovers: ESA Activities for Resource Prospecting at the Poles, in: Annual Meeting of the Lunar Exploration Analysis Group, Vol. 1863 of LPI Contributions, 2015, p. 2027.

[2] M. Anand, Lunar water: A brief review, Earth, Moon, and Planets 107 (1) (2010) 65–73. doi:10.1007/s11038-010-9377-9.
URL https://doi.org/10.1007/s11038-010-9377-9

[3] D. J. Lawrence, W. C. Feldman, R. C. Elphic, J. J. Hagerty, S. Maurice, G. W. McKinney, T. H. Prettyman, Improved modeling of Lunar Prospector neutron spectrometer data: Implications for hydrogen deposits at the lunar poles, Journal of Geophysical Research (Planets) 111 (2006) E08001. doi:10.1029/2005JE002637.

[4] S. J. Barber, I. P. Wright, F. Abernethy, M. Anand, K. R. Dewar, M. Hodges, P. Landsberg, M. R. Leese, G. H. Morgan, A. D. Morse, J. Mortimer, H. M. Sargeant, I. Sheard, S. Sheridan, A. Verchovsky, F. Goesmann, C. Howe, T. Morse, N. Lillywhite, A. Quinn, N. Missaglia, M. Pedrali, P. Reiss, F. Rizzi, A. Rusconi, M. Savoia, A. Zamboni, J. A. Merrifield, E. K. Gibson, J. Carpenter, R. Fisackerly, B. Houdou, E. Sefton-Nash, R. Trautner, ProSPA: Analysis of Lunar Polar Volatiles and ISRU Demonstration on the Moon, in: Lunar and Planetary Science Conference, Vol. 49 of Lunar and Planetary Science Conference, 2018, p. 2172.

[5] M. Formisano, M. C. De Sanctis, S. De Angelis, J. D. Carpenter, PROSPECTing the Moon: Numerical Simulations of Temperature and Sublimation Rate on a Regolith Cylindric Sample, in: Lunar and Planetary Science Conference, Vol. 48 of Lunar and Planetary Science Conference, 2017, p. 1948.

[6] G. H. Heiken, D. T. Vaniman, B. M. French, Lunar sourcebook - A user's guide to the moon, 1991.

[7] K. Ellsworth, G. Schubert, Saturn's icy satellites - Thermal and structural models, Icarus54 (1983) 490–510. doi:10.1016/0019-1035(83)90242-7.

[8] J. Klinger, Influence of a phase transition of ice on the heat and mass balance of comets, Science 209 (1980) 271. doi:10.1126/science.209.4453.271.

[9] A. H. Delsemme, D. C. Miller, The continuum of Comet Burnham (1960 II): The differentiation of a short period comet, Planet. Space. Sci.19 (1971) 1229–1257. doi:10.1016/0032-0633(71)90180-2.

[10] S. Espinasse, J. Klinger, C. Ritz, B. Schmitt, Modeling of the thermal behavior and of the chemical differentiation of cometary nuclei, Icarus 92 (1991) 350–365. doi:10.1016/0019-1035(91)90058-2.

[11] M. T. Capria, F. Capaccioni, A. Coradini, M. C. De Sanctis, S. Espinasse, C. Federico, R. Orosei, M. Salomone, A P/Wirtanen evolution model, Planet. Space. Sci.44 (1996) 987–1000. doi:10.1016/0032-0633(96)00016-5.

[12] J. Lasue, M. C. De Sanctis, A. Coradini, G. Magni, M. T. Capria, D. Turrini, A. C. Levasseur-Regourd, Quasi-3-D model to describe topographic effects on non-spherical comet nucleus evolution, Planet. Space. Sci.56 (2008) 1977–1991. doi:10.1016/j.pss.2008.08.020.

[13] M. C. De Sanctis, J. Lasue, M. T. Capria, G. Magni, D. Turrini, A. Coradini, Shape and obliquity effects on the thermal evolution of the Rosetta

target 67P/Churyumov-Gerasimenko cometary nucleus, Icarus207 (2010a) 341–358. doi:10.1016/j.icarus.2009.11.009.

[14] M. C. De Sanctis, J. Lasue, M. T. Capria, Seasonal Effects on Comet Nuclei Evolution: Activity, Internal Structure, and Dust Mantle Formation, Astron. J.140 (2010b) 1–13. doi:10.1088/0004-6256/140/1/1.

[15] M. Formisano, M. C. De Sanctis, G. Magni, C. Federico, M. T. Capria, Ceres water regime: surface temperature, water sublimation and transient exo(atmo)sphere, MNRAS455 (2016) 1892–1904. doi:10.1093/mnras/stv2344.

[16] M. Formisano, C. Federico, M. C. DeSanctis, A. Frigeri, G. Magni, A. Raponi, F. Tosi, Thermal stability of water ice in ceres' craters: The case of juling crater, Journal of Geophysical Research: Planets 123 (9) (2018) 2445–2463. doi:10.1029/2017JE005417.

[17] M. Formisano, C. Federico, G. Magni, A. Raponi, M. DeSanctis, A. Frigeri, Surface temperatures and water ice sublimation rate of oxo crater: A comparison with juling crater, Journal of Geophysical Research: Planets 0 (0). doi:10.1029/2018JE005839.

[18] F. P. Fanale, J. R. Salvail, The loss and depth of CO2 ice in comet nuclei, Icarus72 (1987) 535–554. doi:10.1016/0019-1035(87)90051-0.

[19] D. M. Murphy, T. Koop, Review of the vapour pressures of ice and supercooled water for atmospheric applications, Quarterly Journal of the Royal Meteorological Society 131 (608) (2005) 1539–1565. doi:10.1256/qj.04.94.
URL http://dx.doi.org/10.1256/qj.04.94

[20] M. Piquette, M. Horányi, S. A. Stern, Laboratory experiments to investigate sublimation rates of water ice in nighttime lunar regolith, Icarus293 (2017) 180–184. doi:10.1016/j.icarus.2017.04.017.

[21] E. L. Andreas, New estimates for the sublimation rate for ice on the moon, Icarus 186 (1) (2007) 24 – 30. doi:https://doi.org/10.1016/j.icarus.2006.08.024.
URL http://www.sciencedirect.com/science/article/pii/S0019103506003046

[22] J. Mortimer, C. Lécuyer, F. Fourel, J. Carpenter, D/H fractionation during sublimation of water ice at low temperatures into a vacuum, Planet. Space. Sci.158 (2018) 25–33. doi:10.1016/j.pss.2018.05.010.

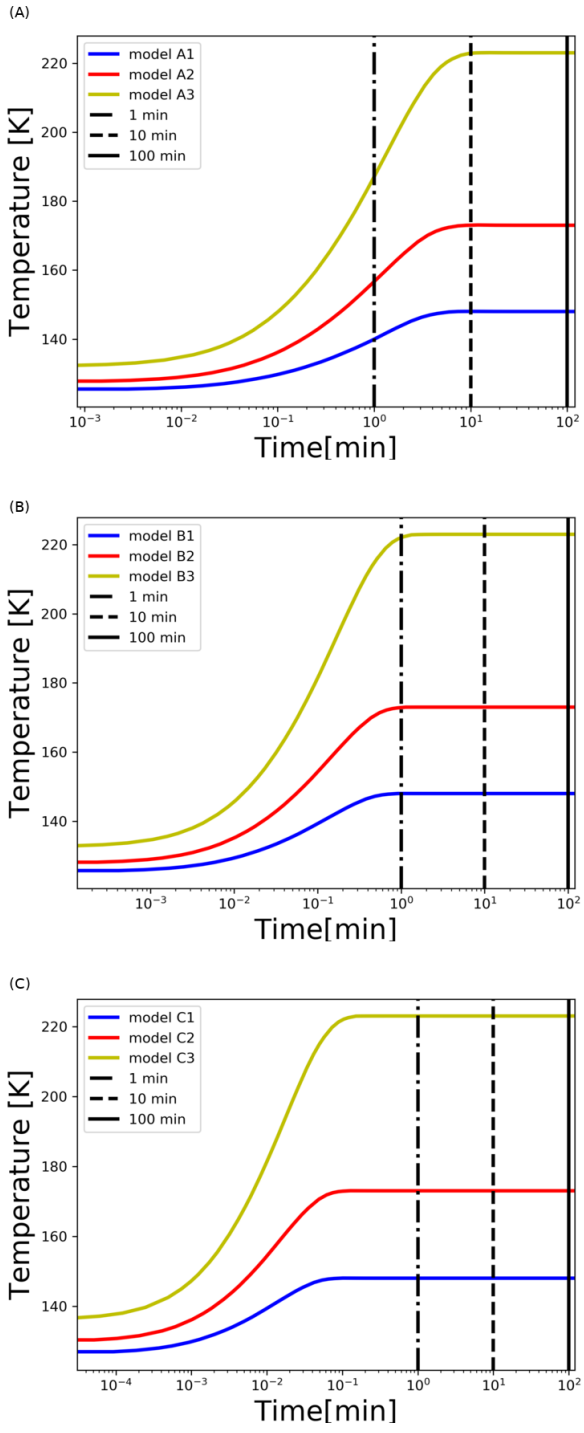

Figure 8: Mean temperature vs time profile for the three scenarios analyzed: (A) Scenario A; (B) Scenario B and (C) Scenario C.